https://doi.org/10.15407/ufm.19.01.025
PACS numbers: 62.20.Qp, 62.25.-g, 68.55.-a, 68.65.Ac, 81.65.Kn

O.V. MAKSAKOVA and O.D. POGREBNJAK
Sumy State University, 2 Rymsky-Korsakov Str., UA-40007 Sumy, Ukraine

V.M. BERESNEV
V.N. Karazin Kharkiv National University, 4 Svobody Sqr.,
UA-61022 Kharkiv, Ukraine

FEATURES OF INVESTIGATIONS OF MULTILAYER NITRIDE COATINGS BASED ON Cr AND Zr

The studies of the structure and properties of nanoscale multilayer coatings of Zr- and Cr-based refractory metals obtained by the vacuum arc cathode deposition are summarized in a brief review of the literature data. A comparative analysis of the microstructure and properties of ZrN/CrN composite coatings depending on the deposition conditions (constant negative potential of the substrate, pulsed high-voltage bias potential, partial pressure, reaction gas velocity) and modulation period for multilayered structure is carried out. General regularities consisting in the presence of the columnar structure and the growth texture are revealed. They show that there is a prevailing (111) orientation for investigated coatings. Conditions for obtaining improved physical, mechanical, and tribological properties of the coatings are determined.

Keywords: multilayer coatings, structure, hardness, corrosion resistance, wear.

Introduction

The scientific and technical interest in the creation of coatings with improved characteristics is associated with the use of new types of multilayer structures with a gradient nature that performs different functions features: adhesive, barrier, wear-resistant, antifriction, *etc.* [1–9]. One of the most promising areas for increasing working characteristics of nitrides *via* their conversion into nanostructured state is a creation of multilayer structures of a nanosize thick [10, 11]. In this case, the alternation of two or more layers of material with different physical and mechanical characteristics can significantly change the properties

of the system, including stress concentration and crack propagation, resulting in an increase in the fracture toughness of the material. Multilayer compositions based on zirconium and chromium nitrides offer a specific interest. The selection of the components for multilayer system is caused by a series of factors. We already know that ZrN films possess a high-energy capacity, the ability to absorb deformation energy and increase the dissipative properties of surface layers, as well as the ability to dissipate effectively deformation energy during the external friction [12, 13]. In addition, the ZrN has a high melting point, Young's modulus, chemical inertness and hardness, good thermal and radiation resistance, as well as thermal shock resistance [14–17]. The CrN films also show oxidation resistance, good wear resistance and high temperature stability [18–22]. However, a single-layer coating of chromium nitride does not have sufficient hardness and is highly susceptible to abrasion [23–26]. The composite compound in the multilayer structure of ZrN and CrN is considered to as a promising, since the high mechanical properties of ZrN are well complemented by the properties of CrN [19, 27, 28].

The goal of this work is to elucidate the current practice and future development trends of multilayer ZrN/CrN systems. Analysis of the results published in scientific and technical literature enabled to determine the regularities of structure formation, the physical, mechanical, and chemical properties of chromium- and zirconium-based layered materials obtained *via* different deposition methods. The review article analyzes the properties of coatings with hardness in the range of 25–55 GPa, combining high chemical, physical, and mechanical properties.

Table 1 comprises state-of-the-art findings of different authors on CrN/ZrN nanostructured physically vapour deposited (PVD) coatings with a thick of bilayers in the range of 2.2–300 nm. One can see from the presented results that hardness of the coatings (H), elastic modulus (E), and other physical and mechanical as well as tribological properties depend on many factors, but first of all on the conditions of the coating formation. Below, we consider in detail data summarized in Table 1.

In the work [34], authors studied an influence of the thickness of bilayers on the microstructural evolution of the coating and their interrelation with mechanical and tribological properties. It is noted that when the thickness of the film decreases, a predominant orientation of the crystallite growth with the [111] axis perpendicular to the growth plane is observed, which is manifested in the relative intensity increase of the corresponding reflex. These results indicate a formation of the superstructure in case of the least layer thickness $\Lambda = 11.7$ nm. Mechanical properties of CrN/ZrN coatings, *viz*. hardness and elastic modulus, are determined by the nanoindentation of the films and amounted 29 GPa and 250 GPa, respectively, while thickness of two nanolayers

varied from 66.7 to 11.7 nm. Tribological tests of the coatings at hand showed that friction coefficient and wear rate (factor) strongly depend on a bilayer thickness. The highest values for these parameters are fixed for the sample with Λ = 11.7 nm: 0.54 and $5.5 \cdot 10^{-7}$ mm^3/Nm, respectively. Consequently, such tribological characteristics make coatings promising for a surface strain hardening of devices.

As a one more example of improving of mechanical and tribological properties of multilayer CrN/ZrN coatings, stands paper [35], where authors analyse effect of bilayer quantity on the morphology, breaking strength, friction coefficient, polarization resistance, and corrosion rate. The correlation between mechanical and microstructural properties of the films was also studied.

The samples were obtained *via* the magnetron sputtering during the same waiting regimes, *i.e.*, the same substrate temperature, pressure, negative bias potential and flux rate relation Ar/N_2, but with different quantities of bilayers: 1, 8, 15 and 30. The atomic force microscope patterns for a surface of the formed coatings showed that films has a substantially high homogeneity, and there no any porosity, delamination, or microdroplet fraction on the surface. Optimal combination of values of the grain size and roughness correspond to the coating with 15 bilayers. Electrochemical behaviour of 3.6% coating in the NaCl solution is investigated by the electrochemical impedance spectroscopy and Tafel polarization curves. The resistance of the samples to corrosion increased with an increase of the number of bilayers due to the quantity of boundaries of alternating CrN and ZrN monolayers and their interaction.

As well as previous papers, article [36] also deals with physical and mechanical properties of CrN/ZrN films and their connection with tribological features. The samples were synthesized *via* magnetron sputtering with unbalanced scheme and change of the rotational velocity for substrate carrier, but with the fixed coating conditions. Chemical elements were distributed over the depth (profiling) using the Auger spectroscopy. Authors [36] revealed that concentration of N, Cr, and Zr components remains unchanged over the all coating thickness. An average value for atomic composition in the films is of the order of (Cr + + Zr)/N = 1. Structural formation of the coatings was determined by the X-ray diffraction. It is stressed that, independently on a rotational velocity of the substrate carrier, the coatings with a preferential (111) orientation are formed. However, these coatings have different level of the internal elastic stresses, *i.e.*, if a bilayer thickness decreases (up to 2.1 nm), the internal compression stresses increase (up to 2.7 GPa). In addition, the sizes of the forming crystals varied within the range of 6.2–9.4 nm depending on the diffraction peak intensities and bilayer thickness. The nanohardness of CrN/ZrN systems, measured *via* the Berkovich indenter, and elastic modulus also increase as compared to

Table 1. **Deposition conditions, characteristics and properties of CrN/ZrN coatings**

Authors	Composition	Method	Deposition parameters
O. Sobol *et al.*, 2016 [29–31]	ZrN/CrN	Vacuum arc deposition	Substrate: steel 12X18H10T, Λ = 20–300 nm, μ = 10 μm, I = 100 A, $P_N = 10^{-5}$–$5 \cdot 10^{-3}$ Torr, –150 V ≤ U_S ≤ –120 V, T_S = 250–350 °C, quantity of layers 12, 24, 564
J.-W. Lee *et al.*, 2013 [32]	CrN/ZrN	Vacuum arc deposition	Substrate: silicon wafers and TiC, Λ = 16 nm, μ = 565–577 nm, I = 70 A, $P_N = 8.6 \cdot 10^{-1}$ Pa, T_S = 150°C, U_S = –100 V
J.-W. Lee *et al.*, 2011 [33]	CrN/ZrN	Vacuum arc deposition	Substrate: silicon wafers and TiC, Λ = 5–30 nm, μ = 511–677 nm, I = 70 A, $P_N = 8.6 \cdot 10^{-1}$ Pa, T_S = 150 °C, U_S = –100 V, grain sizes 2.9–4.69 nm
Z.G. Zhang *et al.*, 2009 [34]	CrN/ZrN	Reaction magnetron sputtering	Substrate: silicon wafers and AISI M2 steel, Λ = 11.7–66.7 nm, μ = 1.9–2.1 μm, $P_N = 5 \cdot 10^{-4}$ Pa, U_S = –60 V, quantity of layers 30–180
N. Sanchez *et al.*, 2008 [35]	CrN/ZrN	High-frequency magnetron sputtering	Substrate: AISI 420 steel, Λ = 100–1000 nm, μ = 3 μm, $P_N = 6.6 \cdot 10^{-3}$ mbar, T_S = 250 °C, U_S = –60 V, grain sizes 39–99 nm, quantity of bilayers 1, 8, 15, and 30
S.-Y. Lee *et al.*, 2008 [36]	CrN/ZrN	Unbalanced magnetron sputtering	Substrate AISI H13 steel, Λ = 2.1–7.1 nm, $P_N = 3.3 \cdot 10^{-3}$ Torr, T_S = 150 °C, U_S = –100 V, grain sizes 6.2–9.4 nm, substrate rotation speed 3, 6, and 15 rpm
D.J. Li *et al.*, 2007 [37]	CrN/ZrN	Magnetron sputtering	Substrate: Si, Λ = 2.2–3.6 nm, μ = 1–1.2 μm, P_N = 0.26 Pa, T_S = 250 °C, U_S = –200 V, substrate rotation 4–11 rpm
D.J. Li *et al.*, 2006 [38, 39]	CrN/ZrN	Dc magnetron sputtering	Substrate: silicon wafers, μ = 800–1000 nm, P_N = 0.28 Pa, T_S = 200 °C, U_S = –200 V, substrate rotation speed 13 rpm
D.J. Li *et al.*, 2004 [40]	CrN/ZrN	Dc magnetron sputtering	Substrate: silicon wafers, P_N = 0.28 Pa

the mononitride CrN coatings (23 GPa and 250 GPa) and reach maximal values of 31.8 and 321.5 GPa, respectively.

Firstly, the multilayer CrN/ZrN structures were obtained in Ref. [40]. Further studies [38–40] report on the considerable improvement of strength characteristics of the coatings using the dc magnetron sputtering. In this way, the multilayer CrN/ZrN films with a nanohardness reaching 55 GPa and failure load of the order of 10^2 mN were synthesized. Such high parameters were reached due to variation of deposition

	Significance of properties	
	tribological	mechanical
		H = 32–42 GPa, E = 210–270 GPa
	Friction coefficient 0.41–0.45, wear factor $3.62 \cdot 10^{-7}$–$4.26 \cdot 10^{-4}$ mm^3/Nm, impact toughness K = 1.85–2.01 MPa·m$^{1/2}$	H = 28 GPa, E = 267 GPa, H_3/E_2 = = 0.11 GPa
	Friction coefficient 0.17±0.05, wear factor $3.62 \cdot 10^{-7}$–$4.26 \cdot 10^{-4}$ mm^3/Nm, impact toughness K = 1.88–2.15 MPa·m$^{1/2}$	H = 25.2 GPa, E = 282 GPa, H_3/E_2 = 0.3 GPa
	Friction coefficient 0.32–0.54, wear factor $5.5 \cdot 10^{-7}$ mm^3/Nm	H = 29 GPa, E = 256 GPa
	Friction coefficient 0.32–0,54	
	Wear factor $0.74 \cdot 10^{-6}$ mm^3/Nm	H = 28.1–31.8 GPa, E = 290–321 GPa, H_3/E_2 = 0.19–0.31
	Failure load 85 mN, wear factor $0.38 \cdot 10^{-5}$ mm^3/Nm	H = 32 GPa
	Failure load 100 mN	H = 48.39–56.47 GPa, E = 381 GPa
		H = 48.39–56.47 GPa, E = 381 GPa

parameters, *viz.* due to reaction gas (N_2 and $N_2 + NH_3$) and its flow rate. Other deposition conditions were as follows: T_S = 200 °C, U_S = –200 V, d_{S-T} = 12 cm, P_{N_2, NH_3} = 0.28 Pa, υ_S = 13 rpm. It is noticed that, if a flow rate of N_2 is 0.6 cm^3/min, the NaCl-type structure coating with a prevailing (111) orientation forms. As the flow-rate value slightly increases up to 0.8 cm^3/min, the preferred orientation is (200). When the value reaches 1 cm^3/min, diffraction reflexes totally disappear. Thus, at a high flow rate of the reaction gas, amorphous nonstoichiometric chro-

mium and zirconium nitrides form. Authors predict that introduction of some amount of NH_3 into the reaction gas during the deposition will contribute to improving the properties of the created coatings. In witness of that, NH_3 was introduced into the deposition chamber. The flow rate of NH_3 was varied from 0.15 to 0.55 cm^3/min, while the flow rate for N_2 was unchanged being equal to 0.6 cm^3/min. The diffraction patterns clearly show significant peak for CrN(111) and weak peaks for ZrN(111), Cr_2N(112), and ZrN(220). Studying of the physical and mechanical properties of the obtained coatings showed that the systems possess increased nanohardness (55 GPa) and elastic modulus (381 GPa) in comparison to the ZrN (22.5 GPa) and CrN (27.5 GPa) mononitride coatings as well as to the CrN/ZrN coatings formed at a flow of N_2 (48.39 GPa). That is why they are especially promising for application as the protective barrier coatings.

The functional properties of nitride coatings depend on their actually created structure (grain size, phase composition, internal stresses, *etc.*); therefore, many researches currently study correlation between structural-phase state and service properties of the coatings depending on methods and conditions of their obtaining. Performing the long-term testing, authors [33] investigated an effect of Cr/Zr relation on mechanical and tribological properties of multilayer CrN/ZrN coatings. The films with different content of chromium and zirconium (1–2.5) were deposited onto the silicon wafer and carbide titanium substrates by the arc-cathode deposition method. Total thickness of the films was the same—circa 16 μm. Optimal conditions for mechanical and adhesion properties (H = 28.8 GPa, E = 267 GPa, K = 1.85 MPa·$m^{1/2}$), high resistance to the plastic deformation (H_3/E_2 = 0.11), and quite well tribological indices (friction coefficient 0.45, wear factor $4.26 \cdot 10^{-4}$ mm^3/Nm) were reached for Cr/Zr equal to 2.7.

Considerable results dealing with possibility of the structural engineering in multilayer arc-vacuum CrN/ZrN coatings were presented by O.V. Sobol *et al*. [29–31]. They established a possibility to reach a superhard state in the multilayer coatings of circa 20 nm thick using the pulsed bias potential. The authors showed the presence of atomic ordering due to the high mobility and decreasing the interboundary mixing in the films. Negative potential results to the formation of solid solutions during deposition due to inter-boundary mixing. Hardness of such systems does not exceed 30 GPa, however in case of an impulse high-voltage action (pulse duration of 10 μs, repetition frequency of 7 kHz, amplitude of 800 V), authors reached a super-hardness effect (up to 42 GPa) at the nanometre-thick layers.

Thus, literature data [29–40] show that chromium- and nitride-based films act as a unique basis for layered materials. They can possess improved physical, chemical, mechanical, and tribological properties

due to the reaching of appropriate functional features, *viz.* (periodic) thickness of the layers, gas atmosphere pressure, and energy factor defined by the bias potential during the deposition.

Below, we go into details of these works [29–40]. We review the structure and properties of the most promising, on our opinion, zirconium- and chromium-nitride-based nanocomposite coatings with different technological conditions during the deposition.

Results and Discussions

Microstructure and Composition of CrN/ZrN Coatings

Analyzing literature data, we established that there are the general regularities and features for given class of coatings in their morphology independently on conditions of the film formations. Figure 1 represents the scanning electron microscopy (SEM) fractographs for surface and lateral cleavage of CrN/ZrN coating with a layer thickness of about 300 nm. There is an insignificant amount of micro-drop fraction on the surface and its practical absence on the cross-section of the coating. The structure demonstrates a sufficiently high homogeneity of the layers along the thickness and quite well planarity.

The high coating continuities and columnar structure are shown in Fig. 2. One can clear see that the coating repeats the substrate surface relief. There were not detected the delaminated or crumbled out coating areas. There is a compact coating structure and clearly observed boundary between the coating and the substrate, which probably should affect the increase of adhesion of the coating and the substrate. The layered structure of films in multilayer structures can remain unbreakable for several millimetres [41–43], which is much more than their extremely small thickness (several nanometres).

The coatings obtained *via* the arc-vacuum deposition methods can have different phase and defect structures. However, their grain structure is represented by columnar crystals, which are directed from transition layer to the coating surface either vertically or angularly to the surface [44–47]. Authors [38] observed columnar microstructure of CrN/ZrN coatings deposited on the silicon substrates by dc magnetron sputtering. In the work [36], the coatings obtained by the unbalanced magnetron sputtering on the steel substrate have a columnar structure as well. Photomicrographs of the lateral section of the CrN/ZrN films obtained by the scanning electron microscopy for lower and higher resolutions are represented in Fig. 3.

Atomic force microscopy (AFM) images for CrN/ZrN coating surfaces (Fig. 4) showed that the compositions have a well-developed, fine-grained surface relief; there are both eminences and valleys. Surface images indicates that depending on bilayer thickness the roughness values

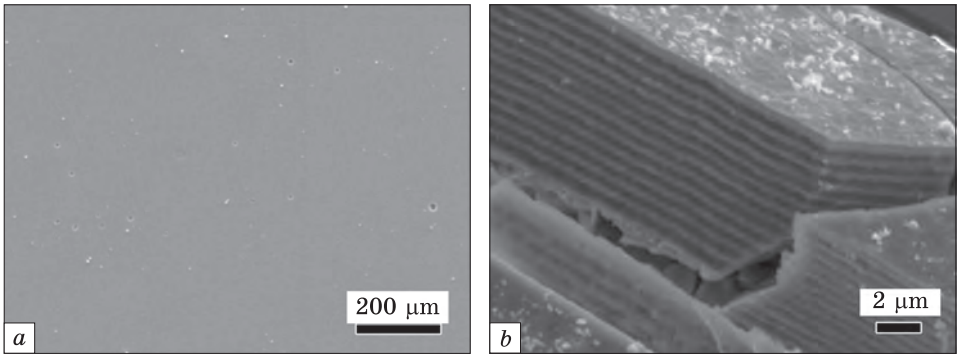

Fig. 1. The scanning electron microscopy (SEM) images of nanocomposite ZrN/CrN coating with a modulation period of 300 nm obtained for surface (*a*) and fracture (*b*) when $P_N = 4 \cdot 10^{-3}$ Torr, $T_S = 250–350$ °C, $U_S = –150$ V [30]

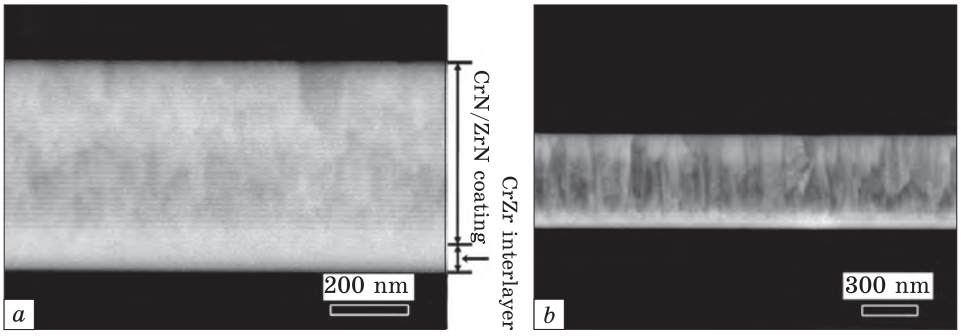

Fig. 2. SEM surface morphologies for the lateral surface of the multilayer CrN/ZrN coatings obtained at $P_N = 8.6 \cdot 10^{-1}$ Pa, $T_S = 150$ °C, $U_S = -100$ V with different bilayer thickness (Λ): 16 nm (*a*) [32] and 6 nm (*b*) [33]

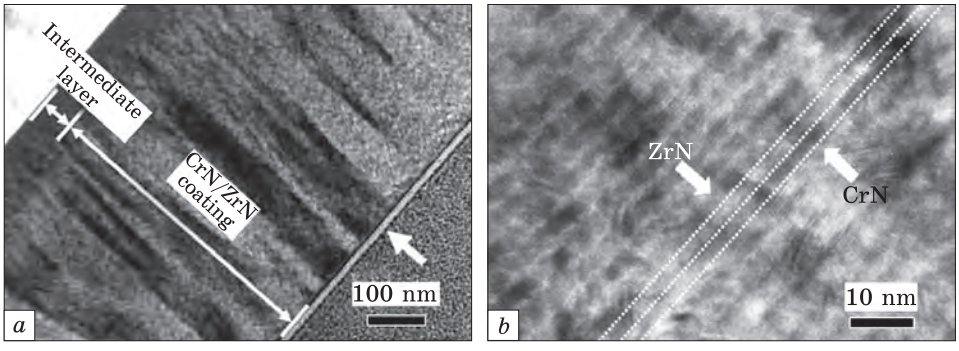

Fig. 3. The cross-sectional transmission electron microscopy (TEM) micrographs of the multilayer CrN/ZrN with bilayer thickness of 5 nm for lower (*a*) and higher (*b*) magnifications [33]

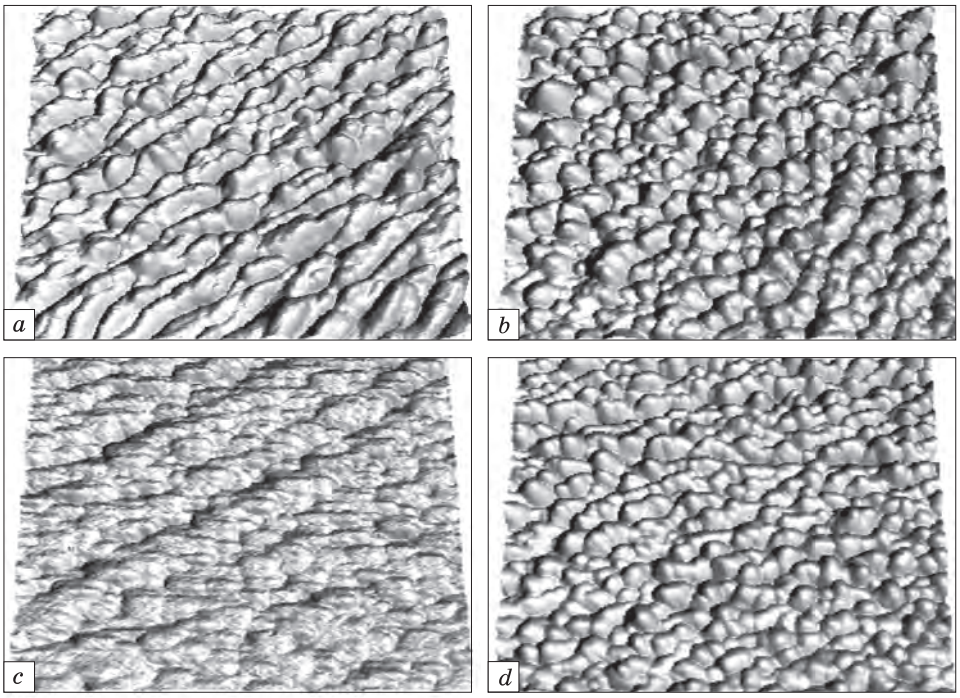

Fig. 4. The 1.0 × 1.0 μm AFM images of CrN/ZrN coatings with bilayer thickness (Λ) of 3 μm (*a*), 375 μm (*b*), 200 nm (*c*), and 100 nm (*d*) [35]

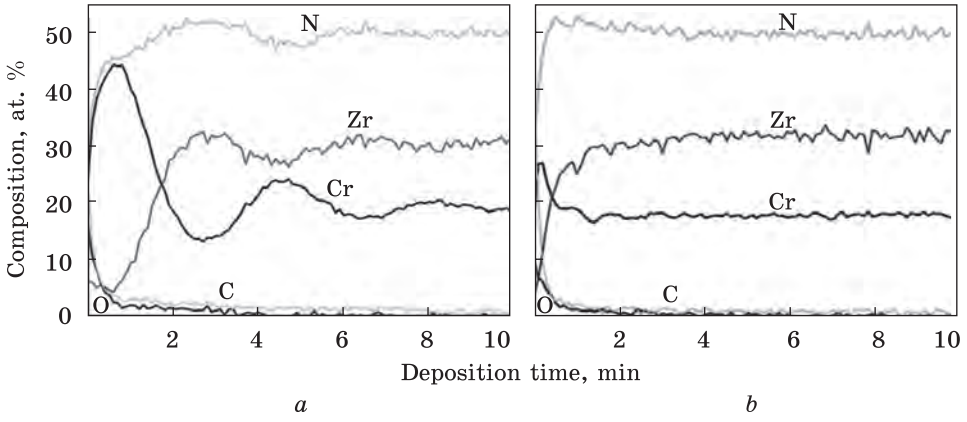

Fig. 5. Composition depth profile for multilayer CrN/ZrN coatings obtained at P_N = = $3.3 \cdot 10^{-3}$ Torr, T_S = 150 °C, U_S = −100 V with different bilayer thickness (Λ): 7.1 nm (*a*) and 2.1 nm (*b*) [36]

vary from 1.9 to 4.4±0.5 nm. Probably relief inhomogeneity is attributed to the presence of macrodefects on the surface and growth of the nitride phase in the coatings [48–50]. Investigations showed that the

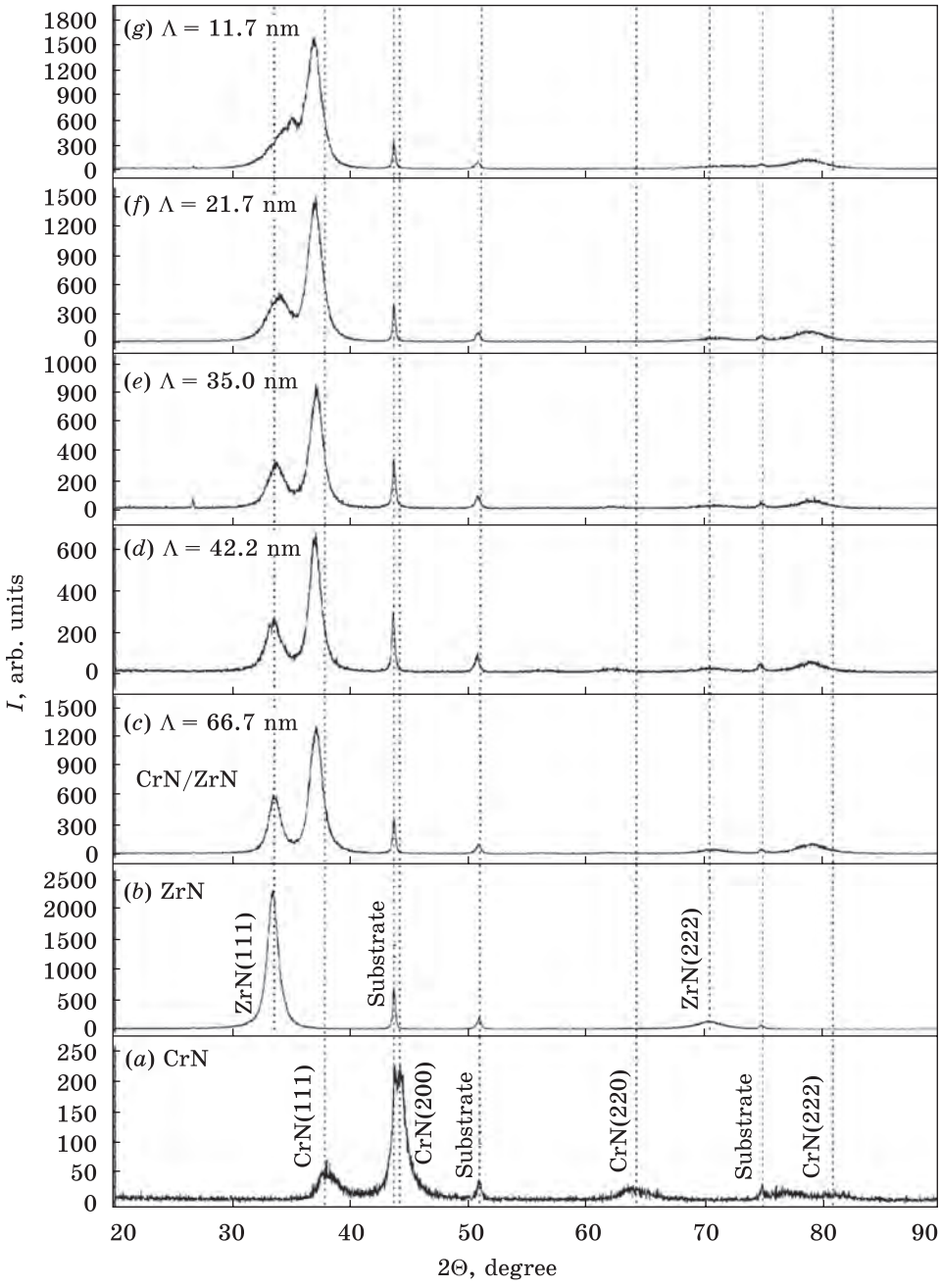

Fig. 6. X-ray diffraction patterns for monolayer CrN and ZrN, as well as multilayer CrN/ZrN coatings obtained at $P_N = 5 \cdot 10^{-4}$ Pa, $U_S = -60$ V [34]

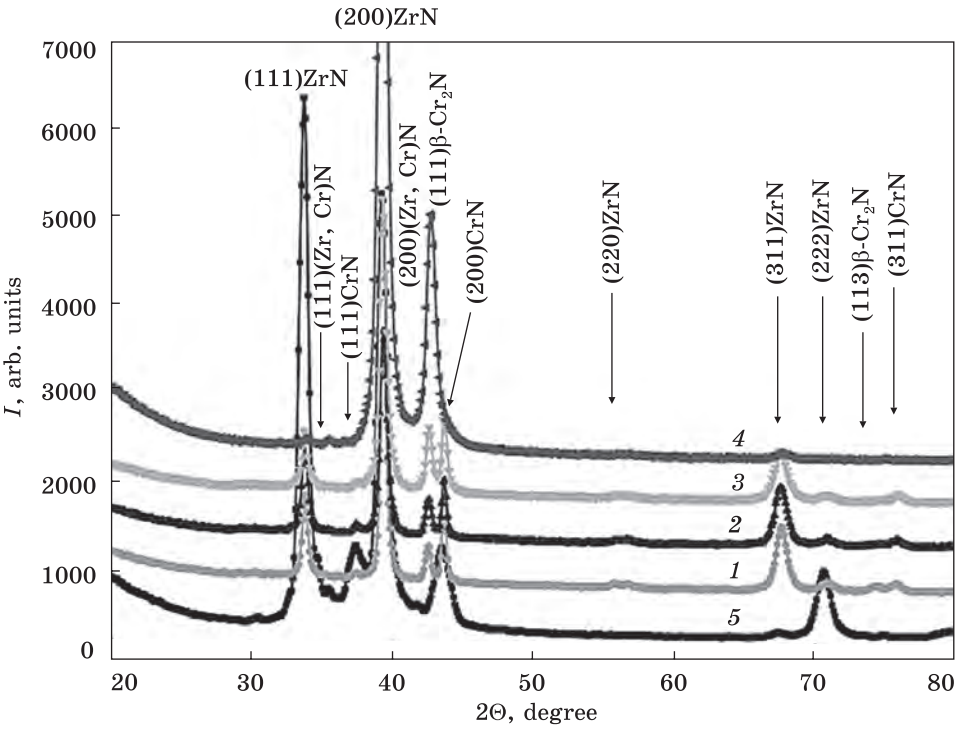

Fig. 7. Regions of diffraction spectra obtained when $P_N = 4 \cdot 10^{-3}$ Torr, $U_S = -150$ V, $U_I = -800$ V for coatings with different bilayer thickness: 300 nm (*1*), 120 nm (*2*), 80 nm (*3*), 40 nm (*4*), and ≈ 20 nm (*5*) [31]

smallest surface roughness, ≈1.9±0.5 nm, is for 100 nm thick bilayer, and the smallest grain size, ≈39±4 nm, is for 375 nm thick bilayer.

The Auger spectroscopy-profiling images (see curves shown in Fig. 5) are the uniform depth distributions of the base elements of the composite multilayer coating.

X-ray diffraction analysis of the structure and phase composition of CrN/ZrN coatings are carried out in typical works [33, 34, 36]. Figure 6 represents X-ray diffraction pattern for multilayer CrN/ZrN samples (with different modulation period) as well as single-layer CrN and ZrN film structures. According to the results for monolayer CrN coating with a *B*1 structure, the preferred plane is (200), and diffraction peaks (111) and (200) have moderate and weak intensity, respectively. The ZrN coatings possess a preferred orientation of (111) and very weak reflection (222). The analysis of X-ray diffraction for monolayer CrN/ZrN film structure revealed formation of the (111) preferred orientation. Based on the intensity of the reflections in the films, one can judge the presence of a critical level of internal stresses, which are typical for the coatings obtained by the arc-vacuum deposition method [30, 51, 52].

As the thickness of bilayers decreases, the reflections for CrN permanently shift to the side of smaller angles. The ZrN (111) diffraction maximum practically is not changeable as the bilayer decreases to 35 nm. With a further decrease in the modulation period, the peak substantially broadens and shifts toward a higher diffraction angle. The observed shift is apparently attributed to decrease in the grain sizes and degree of crystallinity, which agree with Refs. [32, 33].

When bilayer thickness reaches 11.7 nm, the X-ray diffraction pattern shows a preferred CrN with (111) reflection, *i.e.* as the modulation parameter (Λ) decreases, multilayer structure transforms into the 'superlattice structure' state with a single lattice parameter. This is seen from a single peak with satellites on the diffraction pattern. The peak corresponds to d = 2.45 E, which is an average between the interplanar distance $d_{(111)}$ of zirconium nitride and $d_{(111)}$ of chromium nitride. Something like that has already been observed in multilayer structures and it is considered very promising to use multilayer films with ultrathin layers [53, 54].

In a series of works [29–31, 33], the Cr_2N and CrN phases with different proportions appear in the nitride chromium layers. The appearance of such two-phase composition authors [29–31] attribute to impulse high-voltage action applied to the substrate during the arc-vacuum process of the coating formation. The constant negative potential was varied from −70 V to −150 V. According to Ref. [38], the reason for the Cr_2N phase to be arisen is the $N_2 + NH_3$ mixture to be used as a reaction gas. The stoichiometry of coatings also depends on the reaction gas' flow rate. At that, the working pressure in the chamber was circa 0.28 Pa. The regions of the diffraction spectra for such coatings are depicted in Fig. 7.

One can see that for both technologies, the base parameter defining precipitation or absence of the Cr_2N phase is rather an energy factor (defined by the applied bias potential [58, 59]) and working medium than the partial pressure of reaction gas [55–57]. Moreover, as it will be shown further during analysis of the results, the Cr_2N phase can contribute to improving the mechanical properties of the coatings [31, 39].

Taking into account results of all works dealing with the study of multilayer CrN/ZrN coatings, we have to note a substantial dependence of the structure and kinetics of the films' formation on the technological parameters during their formation.

Mechanical Properties of Multilayer CrN/ZrN Coatings

For optimization of the mechanical properties of coatings, the ascertainment of the relationship between the structure and their properties is an important challenge. Hardness is one of the most researched parameters of any coatings, including multi-layer ones.

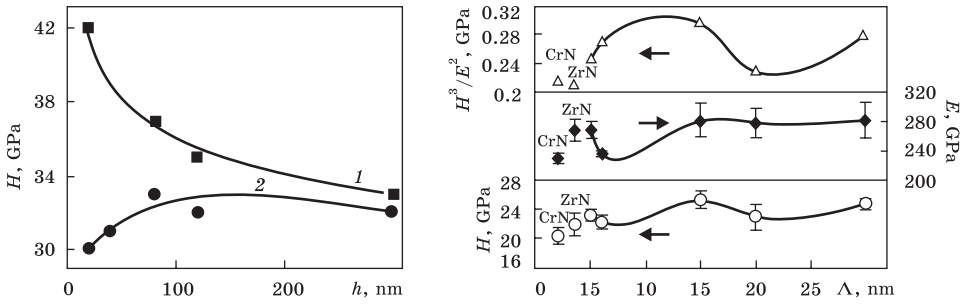

Fig. 8. Dependence of hardness H on the layer thickness h in ZrN/CrN multilayer coating produced at $P_N = 4 \cdot 10^{-3}$ Torr and pulsed stimulation of deposition $U_I = -800$ V for two cases: without (*1*) and with application of a constant voltage $U_S = -150$ V (*2*) [31]

Fig. 9. The hardness (H), elastic modulus (E), and plastic deformation resistance (H^3/E^2) *vs.* the bilayer periods (Λ) for the CrN/ZrN multilayered coatings on Si substrates obtained at $P_N = 8.6 \cdot 10^{-1}$ Pa, $U_S = -100$ V, $T_S = 150$ °C *via* the arc-PVD technique [33]

A relationship between conditions of the deposition process and hardness of CrN/ZrN coating was determined. Within the range of layer thicknesses of 20–300 nm, the maximal value of hardness was circa 42 GPa as Fig. 8 represents. This maximum value corresponds to the coatings produced without a permanent negative bias potential, but with impulse stimulation and the smallest layer thickness of 20 nm. Thus, using of the impulse high-voltage impaction (8% of a total deposition time) for elevation of mobility of deposited atoms does not result to formation of solid-solution phases, probably, due to the possibility of atomic ordering (as in other bulky [60, 61] or plane [62, 63] crystals) during remaining (without impact) time interval (92% of total time). As the negative potential of –70 V and –150 V is applied, the maximal hardness decreases to 33 and 32 GPa, respectively, and the dependence changes its behaviour (Fig. 8). For the smallest thickness (when an influence of potential, which enhances an average energy of deposited particles, on the radiation-stimulated inter-layer mixing is maximal), the lowest values (circa 30 GPa) are reached, while midvalues (about 32–33 GPa) occur at a layer thickness exceeding 100 nm. Note that authors revealed dependence between the hardness and structural characteristics of CrN/ZrN coatings, such as a texture, a crystal lattice parameter, and a size of the crystalline grains.

Thus, the effect of improving mechanical properties with decreasing layer thicknesses to nanometre size in a multilayer composition can be realized in the case of low mixing at the interphase boundary of the layers, which for highly differentiated metal masses composing the multilayer system can be achieved with a low bias potential.

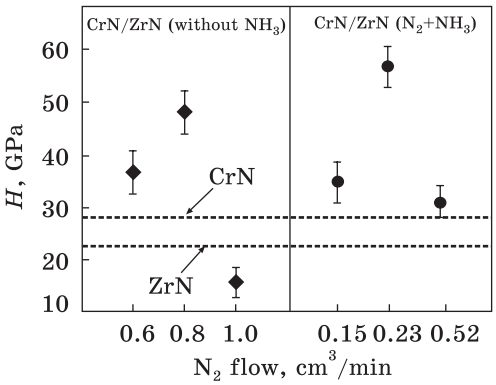

Fig. 10. Nanoindentation hardness (H) *vs.* the flow rate of N_2 and N_2 + NH_3 reaction gases obtained for P_N = = $2.8 \cdot 10^{-1}$ Pa, U_S = –200 V, T_S = = 200 °C *via* dc magnetron sputtering of multilayer CrN/ZrN coatings on Si substrates [38]

According to the findings in the works [32, 33, 36], values of hardness H, elastic modulus E, and plastic deformation H^3/E^2 for CrN/ZrN coatings depend on bilayer thicknesses. Figure 9 represents dependences for these parameters and their comparison with monolayer nitrides. Along with a high hardness, the coatings possess a high elastic modulus. The relation H^3/E^2 characterizes an ability of coating material to counteract to the plastic deformation and is called as the plastic deformation resistance index. The higher value of H^3/E^2, the material is more resistant to the plastic deformation [64–67]. In the range of investigated bilayer thicknesses (Λ = 16–30 nm), the maximal values of hardness (25.2 GPa), elastic modulus (282 GPa), and plastic deformation (0.3 GPa) are observed for Λ = 16 nm. It is well known that hardness, increasing to the maximum value, and then decreasing as the bilayer thickness increases, is a typical phenomenon observed in multilayer coatings [68–70]. In such multilayer systems, the mechanism of hardness increase can be explained by Koehler's theory [71] or the hardening theory [72, 73], which is based on the dislocation blocking at interfaces.

In the works [39, 40], authors estimated mechanical characteristics of coating surfaces *via* determination of nanohardness and elastic modulus as well as their correlation with type of reaction gas and its flow rate during the coating formation. A mixture N_2 + NH_3 acts as a reaction gas, and its delivery rate, when hardness and elastic modulus are maximal (55 and 381 GPa, respectively), is 0.23 cm^3/min (see Fig. 10). These magnitudes 1–1.5 times exceed values of hardness for mononitride CrN and ZrN coatings, and 0.4 times values of hardness obtained by other research groups [34, 36]. There is an explicit dependence of mechanical properties for CrN/ZrN coatings on conditions of their formation. Authors analyze structural-phase state of the coatings and believe that an addition of hydrogen nitride results to increase in crystallinity degree of coatings and formation of nanocrystallites. Thus, the fraction of grain boundaries is also significantly increased. The grain

boundaries in nanocrystalline materials are an obstacle to plastic deformation, which contributes to the hardening of the material [74–76].

Thus, we analyzed the correlation between the parameters in experiments and the hardness of the coatings. From this analysis, we can assert that in order to achieve the maximum hardness of multilayered CrN/ZrN coatings, it is necessary to strive for the formation of a perfect phase structure with the minimum possible grain size and optimal thickness of bilayers.

Corrosion Resistance of Multilayer CrN/ZrN Coatings

The quantitative evaluation of the corrosion resistance of coatings is a difficult problem, since the service life is determined by both the properties of the coating and external conditions.

Work [35] deals with studying of electrochemical properties of multilayer CrN/ZrN coatings produced at P_N = 0.66 Pa, U_S = –60 V, T_S = = 250 °C on the steel substrates by the high-frequency magnetron sputtering technique using electrochemical impedance spectroscopy. Corrosion tests were carried out for 3.5% solution of NaCl at a room temperature. Potentials for samples (E) were measured with respect to silver chloride electrode. Electrode working surface was 1 cm^2. Platinum wafer served as an auxiliary electrode. Impedance measurements were carried out in the potential range ±250 mV. To calculate the corrosion current, the polarization resistance R_p was used *via* the equation [77]

$$I_{\text{cor}} = \frac{\beta_\alpha \beta_c}{2.303 R_p (\beta_\alpha + \beta_c)},$$

where β_α and β_c are the Tafel anode and cathode constants, respectively.

To determine R_p, the current–voltage characteristic near the corrosion potential was measured *via* polarization along cathode and anode directions, while R_p value was calculated by the slope angle of curve at the corrosion potential ($\Delta E \to 0$) [78–80]. Analysis of electrochemical parameters in Table 2 indicates that modulation period of coatings affects on their resistance to corrosion. The Tafel curves presented in Fig. 11 confirm a high corrosion resistance (circa 23 μm/hour).

Figure 12 represents surface images of CrN/ZrN films after

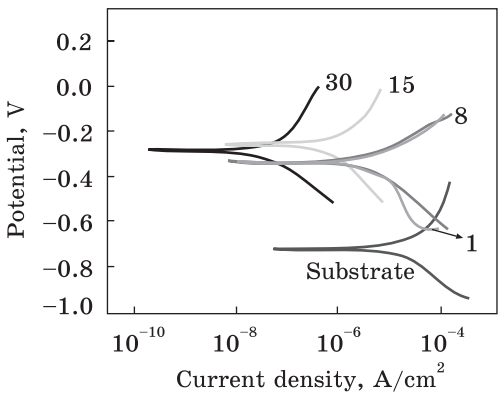

Fig. 11. Tafel polarization curves for CrN/ZrN films with 1, 8, 15, and 30 bilayers [35]

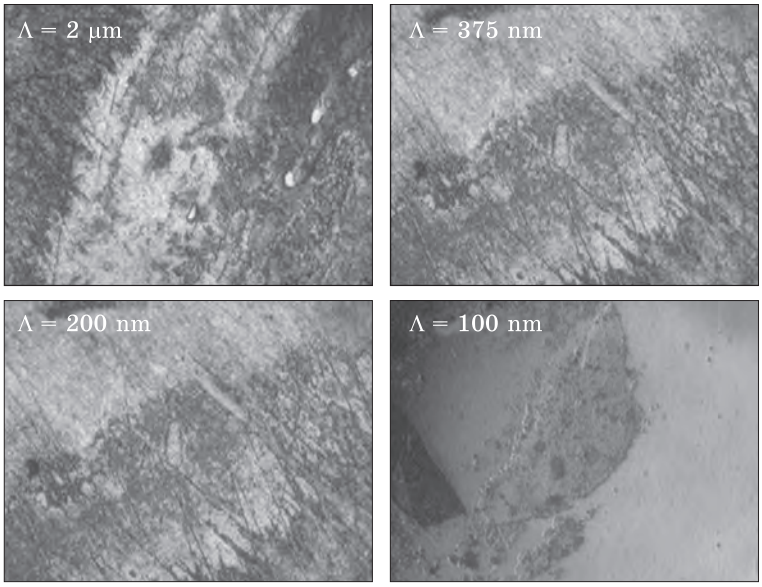

Fig. 12. Micrograph for surface of CrN/ZrN coatings after electrochemical analysis [35]

Table 2. **Electrochemical analysis results of resistance to corrosion for CrN/ZrN coatings in 3.5% water-distilled NaCl solution**

Parameter	Value				
	Substrate	Modulation period			
		3 μm	375 nm	200 nm	100 nm
β_α, V/decade	$496.6 \cdot 10^{-3}$	$128.1 \cdot 10^{-3}$	$132.6 \cdot 10^{-3}$	$323.6 \cdot 10^{-3}$	$62.5 \cdot 10^{-3}$
β_c, V/decade	$270.8 \cdot 10^{-3}$	$190.6 \cdot 10^{-3}$	$185.2 \cdot 10^{-3}$	$540.5 \cdot 10^{-3}$	$102.8 \cdot 10^{-3}$
I_{cor}	40.5	3.74	3.37	1.8	17.6
E_{cor} (mV)	–748	–338	–339	–240	–280
V_{cor}, m/hour	12.43	2.209	2.228	$924.6 \cdot 10^{-3}$	$8.062 \cdot 10^{-3}$

electrochemical tests. As the 100–200 nm thick bilayers get decrease in their thickness, we can observe that corrosion attack does not affect surface of the films. There no considerable changes in these coatings after their subjection to corrosive wear.

Thus, based on the analysis of the corrosion behaviour of CrN/ZrN films in 3.5% aqueous NaCl solution, the corrosion characteristics of the coatings are determined. The relationship between these characteristics and nanometre-thick layers in the multilayer composition is also established.

Tribological Properties of Multilayer CrN/ZrN Coatings

Problems of tribology are discussed in numerous publications in the scientific and technical literature, many aspects of friction and wear processes are considered, however, the number of publications on the friction and wear of nanoscale multilayer CrN/ZrN coatings is currently limited. Tribological characteristics are predictably correlated with the structure of coatings and their mechanical properties. As a rule, coatings with the highest possible hardness and minimum friction coefficient have the lowest wear [81–85].

The authors [38–40] obtained important practical results on friction, wear, and destructive loading. As a deposition method, magnetron

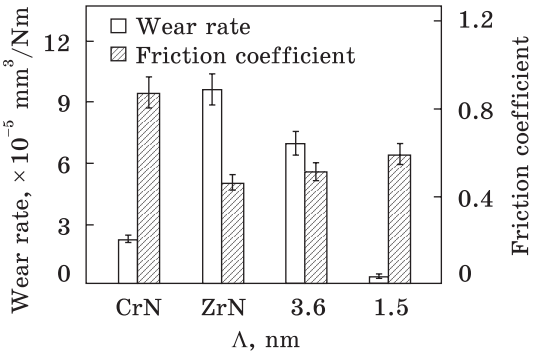

Fig. 13. Wear rate and friction coefficient *vs*. estimated modulation period Λ obtained at $P_N = 2.6 \cdot 10^{-1}$ Pa, $U_S = -200$ V, $T_S = 200$ °C for the CrN/ZrN coatings [37] ►

Fig. 14. Surface profiles of the scratch scan and post scan along with the scratch tracks images of the multilayer CrN/ZrN coatings [39]

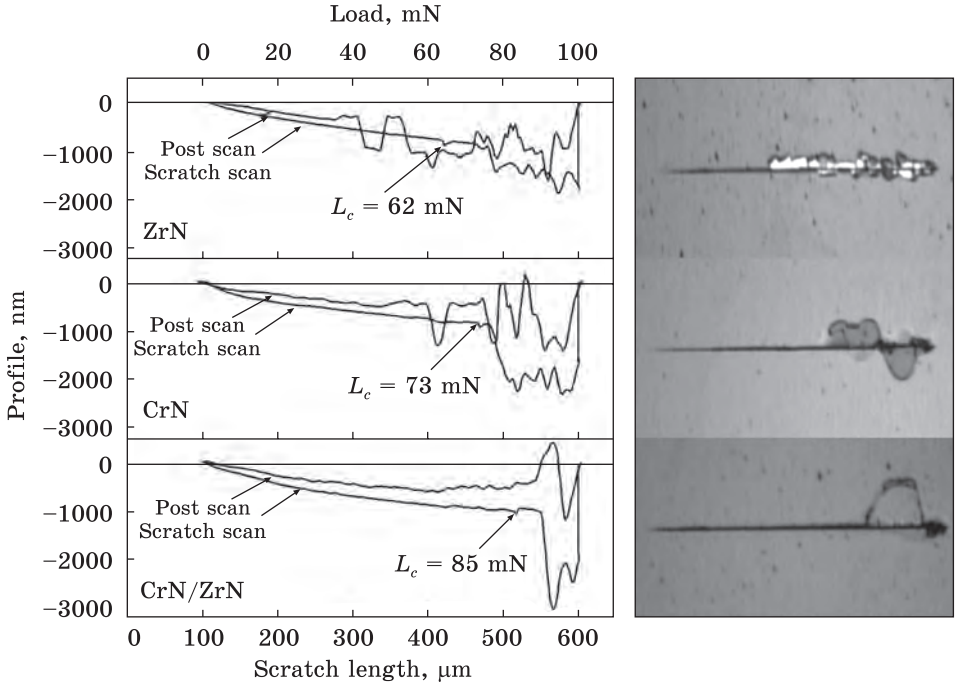

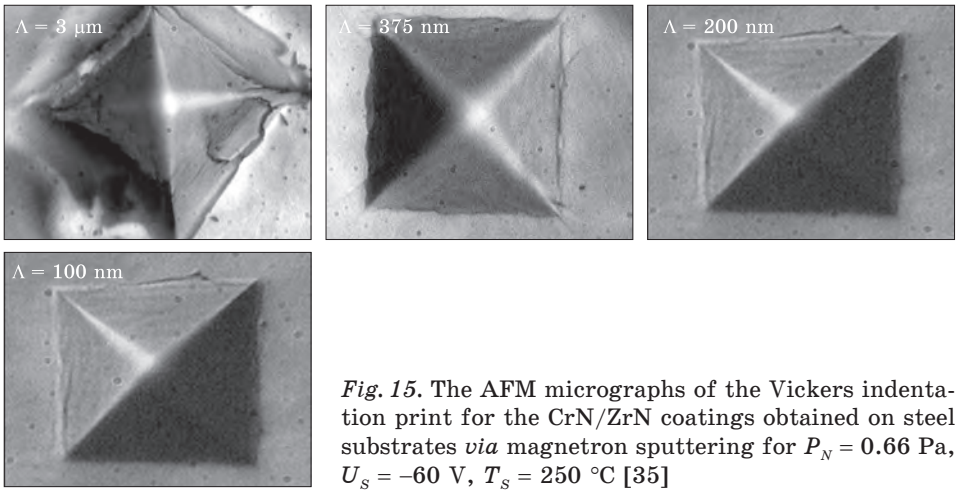

Fig. 15. The AFM micrographs of the Vickers indentation print for the CrN/ZrN coatings obtained on steel substrates *via* magnetron sputtering for $P_N = 0.66$ Pa, $U_S = -60$ V, $T_S = 250$ °C [35]

sputtering at a constant current was used, and silicon wafers served as substrates. Wear measurements were carried out according to the 'ball–disk' scheme at a temperature of 23 °C. As a counter body, a Si_3N_4 ceramic ball was used. The test load was 2 N, and the sliding speed was 1000 rpm. The diameter of the friction track was of 5 mm.

Figure 13 shows dependences of friction coefficient and wear rate for the samples with different modulation period. Measured experimental data indicate that the wear coefficient of multilayer coating with modulation period of 1.5 nm reaches value of $0.3865 \cdot 10^{-5}$ mm^3/Nm that is 6–24 times higher as compared to the value for multilayer CrN and ZrN.

A scratch test was used to analyze the adhesion strength of the coatings that were obtained. The method is based on scratching the surface of the coating when the indenter is loaded uninterruptedly. The research is based on scratching the surface of the coating, under continuous loading of the indenter. The indentation depth was 10–15% of total coating thickness (800 nm–1 μm).

Figure 14 represents a scratch-scan before and after conduction of the tests, as well as images of the coating regions after they were tested. The results are compared with those for the mononitride ZrN and CrN coatings. The first appearance of cracks attributed to cohesive failure of the coating was recorded at loads more than 50 mN. However, it was noted that the appearance of cracks had a single nature. There were no indications of adhesion failure up to the loads greater than 85 mN. The critical load for adhesive failure was 100 mN.

A typical deformation image that occurs in the impression of the Vickers pyramid on the surface of the CrN/ZrN coating is shown in Fig. 15.

Studies of traces of the indenter showed the dependences of resistance to the failure on the modulation period (Λ) in the films. As the thickness of 100–200 nm thick coatings decreases, there is an increasing of failure resistance. Such a result is achieved also due to the layering and nanostructuring of the films.

Thus, despite the fact that the conditions and technologies of the coating depositions differ significantly, we can formulate a general conclusion that the tribological properties of multilayer CrN/ZrN coatings are directly related to the conditions of experimental operations.

Conclusion

Determination of the properties of nitride Cr- and Zr-based multilayer coatings is impossible without reliable identification of their phase and structural states associated with methods and deposition regimes. The enhancement of possibilities and expansion of areas of application of these films is possible *via* optimization of the deposition process, creation of technological conditions for the process of the structural formation of nanoscale films with the required complex of properties. The executed analysis of the structural-phase, mechanical, corrosion, and tribological characteristics of multilayer CrN/ZrN coatings enabled us to make some general conclusions.

• The techniques of formation of multilayer coatings require information on basic parameters determining their structure, phase composition and properties. These parameters are as follows: the value and shape of the applied bias potential, the pressure of the working atmosphere, the selection of the reaction gas and its flow rate. The temperature does not affect substantially the morphology of the compositions.

• We revealed that a decrease in the period of multilayer structures increases their hardness, whose absolute value is determined not only by the phase composition but also by the grain size in the alternate layers, the volume fraction of the interlayer boundaries and the near-boundary areas, the level of internal stresses in the composition and the energy factor during deposition. The hardness of the obtained compositions can be significantly higher in comparison to the hardness of single-layer materials.

• Enhancement of the wear resistance of multilayer systems is associated with a decrease in the friction coefficient, the formation of coatings with a low compressive stresses, sufficiently high hardness, and good adhesion.

The generalized experimental data give a possibility to make a goal-directed influence on the structure, phase composition, as well as physical and mechanical characteristics of coatings, which are one of the most important and promising among current trends in obtaining of new (quasi-two-dimensional) materials.

REFERENCES

1. R.K. Upadhyay and L.A. Kumaraswamidhas, *Surf. Eng.*, **31**, No. 2: 123 (2015).
2. J.N. Ding, Y.G. Meng, and S.Z. Wen, *Thin Solid Films*, **371**, Nos. 1–2: 178 (2000).
3. J. Musil, *Ceram. Eng. Sci. Proc.*, **34**, No. 3: 55 (2014).
4. V.M. Beresnev, O.V. Sobol', A.D. Pogrebnjak, S.S. Grankin, V.A. Stolbovoi, P.V. Turbin, A.A. Meilekhov, and M.Y. Arseenko, *Tech. Phys. Lett.*, **42**, No. 5: 532 (2016).
5. G. Abadias, V.V. Uglov, I.A. Saladukhin, S.V. Zlotski, G. Tolmachova, S.N. Dub, and A.J. van Vuuren, *Surf. Coatings Technol.*, **308**: 158 (2016).
6. A. Pogrebnjak, V. Ivashchenko, O. Bondar, V. Beresnev, O. Sobol, K. Załęski, E. Coy, S. Jurga, P. Konarski, and B. Postolnyi, *Mater. Charact.*, **134**: 55 (2017).
7. V.M. Beresnev, S.A. Klimenko, O.V. Sobol', S.V. Litovchenko, A.D. Pogrebnjak, P.A. Srebnyuk, D.A. Kolesnikov, A.A. Meilekhov, A.A. Postel'nik, and U.S. Nemchenko, *J. Superhard Mater.*, **39**: 172 (2017).
8. B.O. Postolnyi, V.M. Beresnev, G. Abadias, O.V. Bondar, L. Rebouta, J.P. Araujo, and A.D. Pogrebnjak, *J. Alloys and Compounds*, **725**: 1188 (2017).
9. B.A. Latella, B.K. Gan, K.E. Davies, D.R. McKenzie, and D.G. McCulloch, *Surf. Coatings Technol.*, **200**: 3605 (2006).
10. H.C. Barshilia and K. S. Rajam, *Bull. Mater. Sci.*, **26**: 233 (2003).
11. A.D. Pogrebnjak, D. Eyidi, G. Abadias, O.V. Bondar, V.M. Beresnev, and O.V. Sobol, *Int. J. Refract. Met. Hard Mater.*, **48**: 222 (2015).
12. A.L. Kameneva, N.I. Sushenshcov, and A. Klochkov, *Tekhnologiya Metallov*, No. 11: 38 (2010) (in Russian).
13. A.D. Pogrebnjak, A.P. Shpak, V. M. Beresnev, D.A. Kolesnikov, Y.A. Kunitskii, O.V. Sobol, V.V. Uglov, F.F. Komarov, A.P. Shypylenko, N.A. Makhmudov, A.A. Demyanenko, V.S. Baidak, and V.V. Grudnitskii, *J. Nanosci. Nanotechnol.*, **12**, No. 12: 9213 (2012).
14. Z.T. Wu, Z.B. Qi, D.F. Zhang, and Z.C. Wang, *Mater. Lett.*, **164**: 120 (2016).
15. K.A. Gruss, T. Zheleva, R.F. Davis, and T.R. Watkins, *Surf. Coatings Technol.*, **107**, Nos. 2–3: 115 (1998).
16. E. Atar, H. Cimenoglu, and E.S. Kayali, *Key Eng. Mater.*, **280–283**: 1459 (2005).
17. J. Musil, S. Zenkin, Kos, R. Čerstvý, and S. Haviar, *Vacuum*, **131**: 34 (2016).
18. A. Lousa, J. Romero, E. Martínez, J. Esteve, F. Montala, and L. Carreras, *Surf. Coatings Technol.*, **146–147**: 268 (2001).
19. Z.G. Zhang, O. Rapaud, N. Bonasso, D. Mercs, C. Dong, and C. Coddet, *Vacuum*, **82**: 501 (2008).
20. P. Wiecinski, J. Smolik, H. Garbacz, and K.J. Kurzydłowski, *Solid State Phenom.*, **237**: 47 (2015).
21. A. Dasgupta, P.A. Premkumar, F. Lawrence, L. Houben, P. Kuppusami, M. Luysberg, K.S. Nagaraja, and V.S. Raghunathan, *Surf. Coatings Technol.*, **201**, Nos. 3–4: 1401 (2006).
22. D.B. Lee, M.H. Kim, Y.C. Lee, and S.C. Kwon, *Surf. Coatings Technol.*, **141**, Nos. 2–3: 227 (2001).
23. J.L. Mo and M.H. Zhu, *Appl. Surf. Sci.*, **255**, No. 17: 7627 (2009).
24. R.-I. Murakami, Y.-H. Kim, K. Kimura, D. Yonekura, and D.-H. Shin, *JSME Int. Journal, Ser. A: Solid Mech. Mater. Eng.*, **49**, No. 1: 123 (2006).
25. J. Jagielski, A.S. Khanna, J. Kucinski, D.S. Mishra, P. Racolta, P. Sioshansi, E. Tobin, J. Thereska, V. Uglov, T. Vilaithong, J. Viviente, S.Z. Yang, and A. Zalar, *Appl. Surf. Sci.*, **156**, No. 1: 47 (2000).

26. J. Park, P. Kusumah, Y. Kim, K. Kim, K. Kwon, and C.K. Lee, *Electrochemistry*, **82**, No. 8: 658 (2014).
27. I. Milošev, H.-H. Strehblow, and B. Navinšek, *Thin Solid Films*, **303**, Nos. 1–2: 246 (1997).
28. Z.G. Zhang, O. Rapaud, N. Bonasso, D. Mercs, C. Dong, and C. Coddet, *Vacuum*, **82**, No. 11: 1332 (2008).
29. O.V. Sobol, A.A. Andreev, V.F. Gorban, V.A. Stolbovoy, A.A. Meylekhov, A.A. Postelnyk, and A. V. Dolomanov, *Problems of Atomic Science and Technology (PAST)*, **101**, No. 1: 134 (2016).
30. O.V. Sobol, A.A. Andreev, V.F. Gorban, A.A. Meylekhov, H.O. Postelnyk, and V.A. Stolbovoy, *J. Nano- Electron. Phys.*, **8**, No. 1: 01042 (2016).
31. O.V. Sobol', A.A. Andreev, V.F. Gorban', V.A. Stolbovoy, A.A. Meylekhov, and A.A. Postel'nik, *Zhurnal Tekhnicheskoy Fiziki*, **86**, No. 7: 100 (2016) (in Russian).
32. S.F. Chen, Y.C. Kuo, C.J. Wang, S.H. Huang, J.W. Lee, Y.C. Chan, H.W. Chen, J.G. Duh, and T.E. Hsieh, *Surf. Coatings Technol.*, **231**: 247 (2013).
33. S.-H. Huang, S.-F. Chen, Y.-C. Kuo, C.-J. Wang, J.-W. Lee, Y.-C. Chan, H.-W. Chen, J.-G. Duh, and T.-E. Hsieh, *Surf. Coatings Technol.*, **206**, No. 7: 1744 (2011).
34. Z.G. Zhang, O. Rapaud, N. Allain, D. Mercs, M. Baraket, C. Dong, and C. Coddet, *Appl. Surf. Sci.*, **255**, No. 7: 4020 (2009).
35. N.A. de Sánchez, H.E. Jaramillo, Z. Vivas, W. Aperador, C. Amaya, and J.C. Caicedo, *Adv. Mat. Res.*, **38**: 63 (2008).
36. M.-K. Kim, G.-S. Kim, and S.-Y. Lee, *Met. Mater. Int.*, **14**, No. 4: 465 (2008).
37. J.J. Zhang, M.X. Wang, J. Yang, Q.X. Liu, and D.J. Li, *Surf. Coatings Technol.*, **201**, Nos. 9–11: 5186 (2007).
38. D.J. Li, F. Liu, M.X. Wang, J.J. Zhang, and Q.X. Liu, *Thin Solid Films*, **506–507**: 202 (2006).
39. M.X. Wang, J.J. Zhang, Q.X. Liu, and D.J. Li, *Surf. Rev. Lett.*, **13**, Nos. 2–3: 173 (2006).
40. F. Liu, M.X. Wang, Q.X. Liu, and D.J. Li, *Trans. Nonferrous Met. Soc. China*, **14**: 243 (2004).
41. A.D. Pogrebnyak, A.P. Shpak, N.A. Azarenkov, and V.M. Beresnev, *Physics-Uspekhi*, **52**, No. 1: 29 (2009).
42. S. Veprek, M.G.J. Veprek-Heijman, P. Karvankova, and J. Prochazka, *Thin Solid Films*, **476**, No. 1: 1 (2005).
43. A.J. Cavaleiro, A.S. Ramos, R.M.S. Martins, F.M. Braz Fernandes, and M.T. Vieira, *Vacuum*, **139**: 23–25 (2017).
44. G.S. Kim, B.S. Kim, S.Y. Lee, and J.H. Hahn, *Surf. Coatings Technol.*, **200**, Nos. 5–6: 1669 (2005).
45. M. Ohring, *The Materials Science of Thin Films* (Elsevier Inc.: 2013), p. 704.
46. A. Pogrebnjak, V. Rogoz, V. Ivashchenko, O. Bondar, V. Shevchenko, S. Jurga, and E. Coy, *J. Alloys and Compounds*, **718**: 260 (2017).
47. J. Deng, F. Wu, Y. Lian, Y. Xing, and S. Li, *Int. J. Refractory Metals and Hard Materials*, **35**: 10 (2012).
48. A.D. Pogrebnyak, A.G. Ponomarev, A.P. Shpak, and Yu.A. Kunitskii, *Physics-Uspekhi*, **55**, No. 1: 29 (2012).
49. A.D. Pogrebnjak, I.V. Yakushchenko, O.V. Bondar, V.M. Beresnev, K. Oyoshi, O.M. Ivasishin, H. Amekura, Y. Takeda, M. Opielak, and C. Kozak, *J. Alloys and Compounds*, **679**: 155 (2016).

50. A.D. Pogrebnjak, A.A. Bagdasaryan, V.M. Beresnev, U.S. Nyemchenko, V.I. Ivashchenko, Y.O. Kravchenko, Z.H.K. Shaimardanov, S.V. Plotnikov, and O. Maksakova, *Ceram. Int.*, **43**, No. 1: 771 (2017).
51. A.D. Pogrebnjak, O.M. Ivasishin, and V.M. Beresnev, *Uspehi Fiziki Metallov*, **17**: 1 (2016).
52. P.H. Mayrhofer, R. Rachbauer, D. Holec, F. Rovere, and J.M. Schneider, *Protective Transition Metal Nitride Coatings in Comprehensive Materials Processing* (Elsevier Ltd: 2014), p. 355.
53. A. Rizzo, M.A. Signore, M. Penza, M.A. Tagliente, F. De Riccardis, and E. Serra, *Thin Solid Films*, **515**, No. 2: 500 (2006).
54. V.N. Zhitomirsky, I. Grimberg, L. Rapoport, R.L. Boxman, N.A. Travitzky, S. Goldsmith, and B.Z. Weiss, *Surf. Coatings Technol.*, **133–134**: 114 (2000).
55. A.G. Gyglya, I.M. Neklyudov, Uspehi Fiziki Metallov, 6, No. 3: 197 (2005) (in Russian).
56. S.T. Oyama, *The Chemistry of Transition Metal Carbides and Nitrides*, (Springer Netherlands: 1996), p. 1.
57. G. Bertrand, H. Mahdjoub, and C. Meunier, *Surf. Coatings Technol.*, **126**, Nos. 2–3: 199 (2000).
58. F. Noli, P. Misaelides, A. Hatzidimitriou, E. Pavlidou, and A.D. Pogrebnjak, *Appl. Surf. Sci.*, **252**, No. 23: 8043 (2006).
59. S.M. Musameh and S.W. Jodeh, *J. Act. Passiv. Electron. Devices*, **2**: 93 (2007).
60. T.M. Radchenko, V.A. Tatarenko, and S.M. Bokoch, *Metallofizika i Noveishie Tekhnologii*, **28**, No. 12: 1699 (2006); idem, arXiv:1406.0147.
61. T.M. Radchenko and V.A. Tatarenko, *Defect and Diffusion Forum*, **273**: 525 (2008).
62. T.M. Radchenko and V.A. Tatarenko, *Physica E*, **42**, No. 8: 2047 (2010).
63. T.M. Radchenko and V.A. Tatarenko, *Solid State Sciences*, **12**, No. 2: 204 (2010).
64. T.D. Shen, C.C. Koch, T.Y. Tsui, and G.M. Pharr, *J. Mater. Res.*, **10**, No. 11: 2892 (1995).
65. S.-W. Yoon, J.-H. Seo, K.-H. Chae, J.-K. Park, J.-H. Song, V. Jayaram, K.-B. Lee, T.-Y. Seong, and J.-P. Ahn, *J. Nanosci. Nanotechnol.*, **12**, No. 2: 1476 (2012).
66. L. Shan, Y. Wang, J. Li, X. Jiang, and J. Chen, *Tribol. Int.*, **82**: 78 (2015).
67. A.D. Pogrebnjak, A.A. Bagdasaryan, A. Pshyk, and K. Dyadyura, *Physics-Uspekhi*, **60**: 586 (2017).
68. U. Helmersson, S. Todorova, S.A. Barnett, and J. E. Sundgren, *J. Appl. Phys.*, **62**, No. 2: 481 (1987).
69. V.M. Beresnev, O.V. Bondar, B.O. Postol'nyi, M.A. Lisovenko, G. Abadias., P. Chartier, D.A. Kolesnikov, V.N. Borisyuk, B.A. Mukushev, B.R. Zhollybekov, and A.A. Andreev, *J. Frict. Wear*, **35**, No. 5: 374 (2014).
70. A.D. Pogrebnjak, O.V. Bondar, G. Abadias, V. Ivashchenko, O.V. Sobol, S. Jurga, and E. Coy, *Ceram. Int.*, **42**: 11743 (2016).
71. J.S. Koehler, *Phys. Rev. B*, **2**, No. 2: 547 (1970).
72. M. Kato, T. Mori, and L.H. Schwartz, *Acta Metall.*, **28**, No. 3: 285 (1980).
73. R. F. Zhang and S. Veprek, *Mater. Sci. Eng. A*, **424**, Nos. 1–2: 128 (2006).
74. P. Hones, N. Martin, M. Regula, and F. Levy, *J. Phys. D: Appl. Phys.*, **36**, No. 8: 1023 (2003).
75. J. Musil, *Surf. Coatings Technol.*, **207**: 50 (2012).
76. J. Musil, *Surf. Coatings Technol.*, **125**, Nos. 1–3: 322 (2000).
77. M. Stern and A.L. Geary, *J. Electrochem. Soc.*, **104**: 56 (1957).

78. Z. Ahmad, *Principles of Corrosion Engineering and Corrosion Control* (Elsevier Ltd: 2006).
79. M. Zhao, Y. Feng, L. Jiao, H.T. Yuan, X. Zhou, and M.B. Jang, *Int. J. Hydrogen Energy*, **32**, No. 16: 3915 (2007).
80. S. Song and P. Xiao, *Mater. Sci. Eng.: B*, **94**, No. 1: 40 (2002).
81. J.A. Sue and T.P. Chang, *Surf. Coatings Technol.*, **76–77**: 61 (1995).
82. M. Stueber, H. Holleck, H. Leiste, K. Seemann, S. Ulrich, and C. Ziebert, *J. Alloys and Compounds*, **483**, Nos. 1–2: 321 (2009).
83. A. Rizzo, M. A. Signore, D. Valerini, D. Altamura, A. Cappello, and L. Tapfer, *Surf. Coatings Technol.*, **206**, No. 10: 2711 (2012).
84. I.V. Blinkov, A.O. Volkhonskiy, V.N. Anikin, M.I. Petrzhik, and D.E. Derevtsova, *Physics and Chemistry of Materials Treatment*, No. 4: 37 (2010).
85. M. Uchida, N. Nihira, A. Mitsuo, K. Toyoda, K. Kubota, and T. Aizawa, *Surf. Coatings Technol.*, **177–178**: 627 (2004).

Received November 28, 2017;
in final version, March 26, 2018

О.В. Максакова, О.Д. Погребняк
Сумський державний університет,
вул. Римського-Корсакова, 2, 40007 Суми, Україна
Sumy State University, 2 Rymsky-Korsakov Str., UA-40007 Sumy, Ukraine

В.М. Береснєв
Харківський національний університет імені В.Н. Каразіна,
пл. Свободи, 4, 61022 Харків, Україна

ОСОБЛИВОСТІ ДОСЛІДЖЕНЬ БАГАТОШАРОВИХ НІТРИДНИХ ПОКРИТТІВ НА ОСНОВІ Cr І Zr

У короткому огляді літературних даних узагальнено результати досліджень структури та властивостей наномасштабних багатошарових покриттів тяжкотопких металів на основі Zr та Cr, одержаних методами вакуумно-дугового осадження катоди. Проведено порівняльну аналізу мікроструктури та властивостей композиційних покриттів ZrN/CrN, залежно від умов осадження (постійного негативного потенціялу підложжя, імпульсного високовольтного потенціялу зміщення, парціяльного тиску, швидкости потоку робочого газу) та періоду модуляції багатошарової структури. Виявлено загальні закономірності, що полягають у наявності стовпчастої структури та текстури росту. Показано, що для досліджуваних покриттів має місце переважна орієнтація (111). Визначено умови одержання поліпшених фізико-механічних і трибологічних властивостей покриттів.

Ключові слова: багатошарові покриття, структура, твердість, корозійна стійкість, зношування.

О.В. Максакова, О.Д. Погребняк,
Сумский государственный университет,
ул. Римского-Корсакова, 2, 40007 Сумы, Украина

В.М. Береснєв
Харьковский национальный университет имени В.Н. Каразина,
пл. Свободы, 4, 61022 Харьков, Украина

ОСОБЕННОСТИ ИССЛЕДОВАНИЙ МНОГОСЛОЙНЫХ НИТРИДНЫХ ПОКРЫТИЙ НА ОСНОВЕ Cr И Zr

В кратком обзоре литературных данных обобщены результаты исследований структуры и свойств наномасштабных многослойных покрытий нитридов тугоплавких металлов на основе Zr и Cr, полученных методами вакуумно-дугового осаждения катода. Проведён сравнительный анализ микроструктуры и свойств композиционных покрытий ZrN/CrN в зависимости от условий осаждения (постоянного или импульсного отрицательного потенциала подложки, импульсного высоковольтного потенциала смещения, парциального давления, скорости потока рабочего газа) и периода модуляции многослойной структуры. Выявлены общие закономерности, состоящие в наличии столбчатой структуры и текстуры роста. Показано, что для исследуемых покрытий имеет место преимущественная ориентация (111). Установлены условия получения улучшенных физико-механических и трибологических характеристик покрытий.

Ключевые слова: многослойные покрытия, структура, твердость, коррозионная стойкость, износ.